GFD 2017 Lecture 4: Processes at the Ice-Ocean Interface

Andrew Fowler; notes by Margaret Lindeman, Agostino Meroni, and Earle Wilson

June 22, 2017

1 Ice Streams and Ice Shelves

1.1 Ice Streams

Ice streams are channels of fast flow within an ice sheet. These frozen rivers of ice provide the main drainage pathways for the large masses of ice that accumulate on Greenland and Antarctica. Since ice streams typically flow orders of magnitude faster than the surrounding ice sheet, they are usually delineated by elongated crevasses. Notable examples of ice streams are the Jakobshavn glacier in West Greenland, which flows at a mean rate of 15 kilometers per year, and the Siple Coast ice streams in Antarctica, which have undergone rapid retreat over the past century.

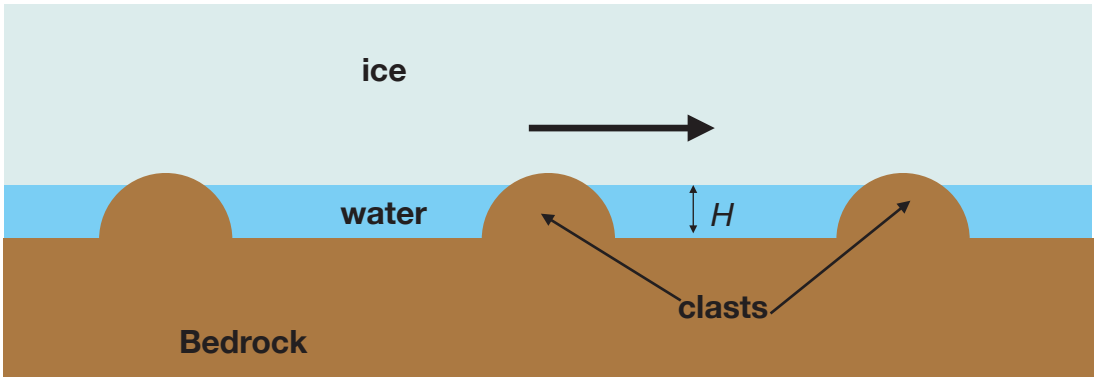

Figure 1: A schematic showing a cross-sectional view of an ice-sheet flowing over bedrock. This schematic is an adaption of Figure 1 in Kyrke-Smith et al. (2013).

Figure 1 provides a simplified cross-sectional view of an ice sheet sliding over bedrock. Here, the ice sheet slides on top of rigid clasts that provide an opposing frictional drag. Between the ice sheet and bedrock is a thin layer of meltwater that has thickness H. The

shear stress at the base of this ice-stream is modeled using the sliding law

$$\tau_b = c\,|u_b|^p\,N^q\,\frac{u_b}{|u_b|}, \tag{1}$$

where τ_b is the basal stress, c is a measure of effective roughness, u_b is the basal velocity, N is the effective pressure, and p and q are positive. The effective pressure is defined as $N = p_i - p_w$, where p_i is the ice pressure and p_w is the basal water pressure. As the water level increases, the points of contact between the ice and the bedrock decreases. Thus, N should decrease with H. Once the ice is lifted above the highest clasts, it will experience much less resistance from the bedrock and flow much more freely. Further increases to the meltwater thickness will have a relatively small effect on the effective pressure. We can therefore identify two distinct states of ice sheet flow: one where the ice is in full contact with bed and N is strongly dependent on water film thickness, and another where the ice is essentially floating on top of meltwater and experiences very little frictional drag.

Mass conservation for the meltwater layer takes the form

$$\frac{\partial H}{\partial t} + \nabla\,\cdot\,\mathbf{q} = \Gamma, \tag{2}$$

where $\mathbf{q}$ is the water flux and Γ is the water source due to basal melting. Assuming a local Poiseuille flow, the meltwater flux $\mathbf{q}$ is given by

$$\mathbf{q} = -\frac{h^3}{12\,\eta_w}\,\nabla\,\psi = \frac{h^3}{12\,\eta_w}\,(-\rho_i\,g\,\nabla s_i - \Delta\rho_{wi}\,g\,\nabla s_w + \nabla\,N), \tag{3}$$

where ψ is the hydraulic potential of the water film, η_w is the viscosity of water, ρ_i is the density of ice and $\Delta\,\rho_{wi} = \rho_w - \rho_i$ is the difference between water density and ice density. The melt rate is given by

$$\Gamma = \frac{G\,+\,\mathbf{u_b}\cdot\tau_\mathbf{b} - q_T + |\mathbf{q}\cdot\nabla\psi|}{\rho_w\,L}. \tag{4}$$

where G is the geothermal heat flux, $\mathbf{u_b}\cdot\tau_\mathbf{b}$ is the work done by the ice on its bed, q_T is the sensible heat loss to the overlying ice and $|\mathbf{q}\cdot\nabla\psi|$ is the heating due to viscous dissipation. Equations (1)-(4) reveal the potential for a positive feedback between ice-velocity and basal heating whereby a positive perturbation in the flow field leads to an increase in basal heating and a decrease in effective pressure. With lower effective pressure the ice is able to slide faster, which then leads to more basal heating and meltwater production. This cycle of amplification is known as *hydraulic runaway*.

For a more thorough discussion on the dynamics of ice streams and hydraulic runaway, the reader is referred to Kyrke-Smith et al. (2013). For more details on the drainage of subglacial water sheets, the reader is referred to Creyts and Schoof (2009).

1.2 Ice shelves

When an ice sheet reaches the ocean, it may begin to float as it continues to flow outward, forming an ice shelf. The scales and dynamics of an ice shelf are distinct from those of the ice sheet.

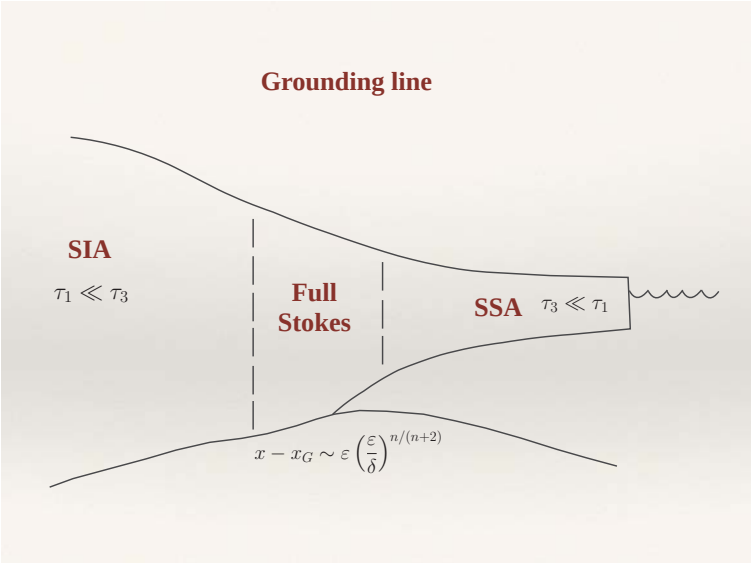

Figure 2: Schematic of grounding line dynamics. The shallow ice approximation (SIA) is applicable to the ice sheet upstream of the grounding line, while the shallow shelf approximation (SSA) is applied to the ice shelf. The grounding line region width is given by (15).

To model the ice sheet, we previously referred to the shallow ice approximation (SIA), with aspect ratio

$$\epsilon = \frac{d}{l} \ll 1. \tag{5}$$

The dominant balance in this approximation was between shear stress τ_3 and horizontal pressure gradient, taking longitudinal stress τ_1 to be negligible (e.g. Meur et al. (2004); Kirchner et al. (2016); figure 2).

Now we will use the shallow shelf approximation (SSA). As the name suggests, the aspect ratio is the same, but now the dominant balance is between the horizontal pressure gradient and longitudinal stress τ_1 (figure 2). This requires a rescaling of the equations in order to apply them to the ice shelf. To this end, we introduce a parameter,

$$\delta = \frac{\rho_w - \rho_i}{\rho_i}, \tag{6}$$

such that we can define a scaling for the ice shelf depth,

$$\nu = \frac{\epsilon}{\delta}\left(\frac{\delta}{\lambda}\right)^{1/(n+1)}, \tag{7}$$

where the ice shelf length scale is given by λ.

Making the assumption that velocity is purely horizontal and varies only in the along-flow direction x, we get the following equations for ice velocity in the SSA:

$$u = \{\tfrac{1}{2}(n+1)(\tfrac{1}{4}q_I)\}^{1/(n+1)}(x - x_G)^{1/(n+1)}, \tag{8}$$
$$u_x = \tfrac{1}{2}(\tfrac{1}{4}H)^n. \tag{9}$$

Defining the ice height at the grounding line x_G as H, we also have an expression for ice flux to the ice shelf at the grounding line,

$$q_I = Hu. \tag{10}$$

2 Grounding Line Dynamics, Calving and Tidewater Glaciers

2.1 The grounding line

To determine q_I and the location of the grounding line x_G, we need to solve a boundary layer problem where we match the SIA and the SSA through a transitional region where neither approximation is applicable.

First, recall these governing equations for inland ice sheet flow:

$$H = s - b, \tag{11}$$
$$H_t + q_x = a, \tag{12}$$
$$q = \frac{H^{n+2}|s_x|^{n+1}(-s_x)}{n+2}, \tag{13}$$

where H is the depth of the ice, q is the ice flux, and (12) is an expression of mass conservation. To match the two sides of the grounding line, we take the boundary conditions as $x \to x_G$ to be (at leading order)

$$H \to 0, \quad q \to q_G, \tag{14}$$

where q_G is the ice flux from the ice sheet. These conditions describe a point-sink at the grounding line. (Note that in steady state, $q_I = q_G$. However, in an unsteady state, the grounding line can move, such that q_I and q_G are related by (36).)

The full Stokes equations can be used to describe the dynamics of the transition region surrounding the grounding line, the width of which scales as

$$x - x_G \sim \epsilon\left(\frac{\epsilon}{\delta}\right)^{n/(n+2)}. \tag{15}$$

Rescaling the variables for the transition zone, we redefine a coordinate system where the grounding line is at $X = 0$, and derive the following matching condition for the ice surface as $X \to -\infty$:

$$S \sim -\lambda X, \tag{16}$$

$$\lambda = \frac{\{(n+2)q_G\}^{1/n}}{(-B_G)^{(n+2)/n}}. \tag{17}$$

The rescaled model for incompressible Stokes flow in the transition zone where $\Pi = P + S$ is

$$U_X + W_Z = 0. \tag{18}$$

$$\Pi_X = T_{3Z} + T_{1X}, \tag{19}$$

$$\Pi_Z = -T_{1Z} + T_{3X}, \tag{20}$$

$$U_Z + W_X = T^{n-1}T_3, \tag{21}$$

$$2U_X = T^{n-1}T_1, \tag{22}$$

$$T^2 = T_3^2 + T_1^2. \tag{23}$$

The boundary conditions on the surface ($Z = 0$ in the scaled coordinates) are

$$T_3 = W = 0. \tag{24}$$

The base of the floating ice is a free boundary ($Z = B$, $X > 0$), with boundary conditions

$$B = -(\Pi + T_1 + T_3 B_X), \tag{25}$$

$$T_3(1 - B_X^2) = 2T_1 B_X, \tag{26}$$

$$W = (-\dot{x}_G + U)B_X, \tag{27}$$

where $\dot{x}_G = \frac{\mathrm{d}}{\mathrm{d}t^*}x_G$ (and t^* is rescaled time). The boundary conditions on the grounded base ($Z = B_G$, $X < 0$) are

$$W = 0, \tag{28}$$

$$T_3 = \beta U, \tag{29}$$

where (29) is a sliding law with basal sliding parameter β.

Now, we will define the necessary conditions to match between the three regions. For the ice sheet (SIA), the matching conditions as $X \to -\infty$ are

$$\Pi_X \to -\lambda, \tag{30}$$

$$W \to 0, \tag{31}$$

$$T_3 \to -\lambda Z. \tag{32}$$

For the ice shelf (SSA), the matching conditions as $X \to \infty$ are

$$T_1 \sim -\tfrac{1}{4}B, \tag{33}$$

$$B \sim -\frac{q_I}{U}, \tag{34}$$

$$U \sim [\tfrac{1}{2}(n+1)(\tfrac{1}{4}q_I)^n X]^{1/(n+1)}. \tag{35}$$

Mass flux to the ice shelf, q_I, is defined by

$$q_I = q_G + \dot{x}_G B_G. \tag{36}$$

The surface is defined as

$$S = (\Pi + T_1)\Big|_{Z=0}. \tag{37}$$

It should be possible to determine B from (27), but $\dot{x}_G$ is still unknown.

To address this, we introduce physically straightforward contact conditions. We require a downward normal stress upstream of the grounding line ($X < 0$):

$$B + \Pi + T_1 > 0. \tag{38}$$

Downstream of the grounding line ($X > 0$), we require that the base of the ice be floating:

$$B > B_G. \tag{39}$$

Finally, at the grounding line ($X = 0$), the effective normal stress is zero, allowing the ice to lift off of the bed:

$$B + \Pi + T_1 = 0. \tag{40}$$

Numerical solutions suggest that there is a unique value of ice flux from the ice sheet at the grounding line, q_G, (proportional to λ^n) that satisfies the contact conditions:

$$q_G = \frac{\lambda^n H_G^{n+2}}{n+2}, \tag{41}$$

where H_G is the grounding line ice thickness.

2.1.1 Marine ice sheet instability

A marine ice sheet, which is grounded below sea level, may become unstable if its bed slopes downwards inland (Fowler, 2011). The dynamics of this instability, which is known as the marine ice sheet instability (MISI), is described in Figure 3. Here, the delivered ice flux, q_0, is assumed to be a linear function of distance and proportional to snow accumulation. The grounding line ice flux, q_G, is an increasing function of ice depth, as in (41).

In the example shown in figure 3, the slope of the bed depth below sea level, H_G, changes sign twice, so there are three intersections between q_0 and q_G. Such an equilibrium is unstable where $\frac{\partial q_0}{\partial x}$ is greater than $\frac{\partial q_G}{\partial x}$, so A and

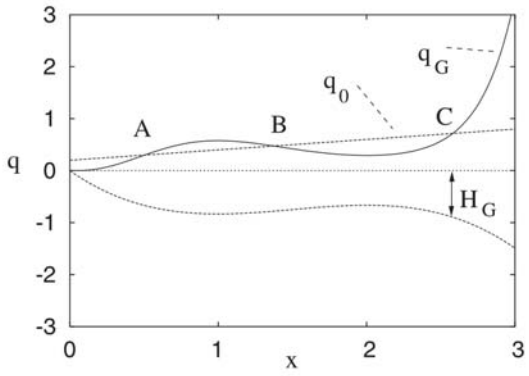

Figure 3: Schematic of MISI. q_0 is the delivered ice flux, q_G is the grounding line flux, H_G is the depth of the bed below sea level, and A, B, and C are the equilibrium positions.

C are stable, while B is unstable. Intuitively, this makes sense, because if the grounding line x_G advances from B, the delivered flux q_0 ex-ceeds the flux through the grounding line q_G, causing the x_G to advance until it reaches the next stable equilibrium, C. Conversely, if xG is perturbed in the opposite direction, retreat-ing from B, qG exceeds q0, resulting in unabated retreat until A is reached. In contrast, the ice sheet recovers from small perturbations in either direction at A or C.

2.2 Calving

The process of calving refers to the fracture of an ice-shelf or a glacier terminus in the sea. Iceberg calving is a sink in the overall ice sheet mass balance and it has been observed to be especially important in Antarctica. In particular, there are circumstances in which glaciers can undergo rapid ice loss through iceberg calving, and these events can have a significant impact on global sea level. Due to the complexity of the phenomena involved and the danger inherent in making observations near a calving face, there is still not a complete and thorough theory describing calving.

2.2.1 Calving mechanisms

Consider a tidewater glacier and let h_i be the thickness of the ice and h_w be the depth of the water. By scaling the momentum equation along x on an ice shelf, one finds that the net balance is between the longitudinal shear stress term and the pressure gradient term, namely

$$\frac{\partial \tau_{11}}{\partial x} = \frac{\partial p}{\partial x}. \tag{42}$$

By integrating the above equation along x across the interface

$$\tau_{11} = p_i - p_w, \tag{43}$$

and integrating over the depth, one gets

$$h_i \overline{\tau_{11}} = \frac{g}{2}\left(\rho_i h_i^2 - \rho_w h_w^2\right), \tag{44}$$

where the overbar denotes vertical average, g is the acceleration due to gravity and ρ_i and ρ_w are ice and water density, respectively. This leads to

$$\overline{\tau_{11}} = \frac{\rho_i g h_i}{2}\left(1 - \frac{\rho_w h_w^2}{\rho_i h_i^2}\right), \tag{45}$$

indicating that if the pressure jump at the interface balances the depth integrated longitudinal stress, the calving front is in equilibrium. Whether the ice is grounded ($\rho_i h_i > \rho_w h_w$) or floating ($\rho_i h_i = \rho_w h_w$), $\bar{\tau_{11}}$ is greater than 0. In the case that $\bar{\tau_{11}}$ exceeds the yield stress, the ice may fracture.

In particular, calving occurs when fractures propagate to a suffucient depth to isolate blocks from the main glacier mass. Nye (1957) suggested that the crevasses penetrate to a depth d where a balance between the tensile strain rate and the creep closure rate due to the hydrostatic pressure is reached, namely

$$d = \frac{2}{\rho_i g}\left(\frac{\dot{\epsilon}}{A}\right)^{1/n}, \tag{46}$$

where A and n come from the Glen's flow law, which relates the strain rate $\dot{\epsilon}_{ij}$ to the stress tensor τ_{ij} as $\dot{\epsilon}_{ij} = A\tau^{n-1}\tau_{ij}$. The presence of meltwater in the crevasses can help to deepen them because of the additional hydrostatic water pressure. In Nye's model this is accounted for as

$$d = \frac{2}{\rho_i g}\left[\left(\frac{\dot{\epsilon}}{A}\right)^{1/n} + \rho_w g d_w\right], \tag{47}$$

where d_w is the water column depth in the crevasse.

Benn et al. (2007) affirm that the four major mechanisms that control calving are, in order of importance:

1. *stretching in response to large-scale velocity gradients*: the velocity distribution at the ice surface is a primary control on the crevasse depth, which is enhanced by meltwater, and the calving margin, which is also influenced by the ice cliff height;
2. *force imbalances at an unsupported ice cliff;*
3. *undercutting of the ice cliff by melting at the submerged ice interface*; and
4. *torque arising from buoyant forces.*

2.2.2 Calving laws

In the literature there have been multiple attempts to quantify the calving rate as a function of other ice or ocean parameters. While no calving laws have yet been established for ice shelves, for tidewater glaciers the rate of change of the ice front position $\dot{x}_s$ has been related to the calving rate u_c through

$$\dot{x}_s = \overline{u} - u_c, \tag{48}$$

where $\overline{u}$ is the vertically averaged glacier velocity at the terminus (Benn et al., 2007). Multiple works, such as Haresign (2004); Benn et al. (2007), have shown that an empirical linear law links the calving rate to the height of the water column at the terminus as

$$u_c = a + bh_w. \tag{49}$$

Although the behavior seems to be quite universal, the coefficients a and b have been found to be glacier- and time-dependent (seasonally). In addition, calving rates of freshwater-terminating glaciers are around one order of magnitude lower than tidewater glacier calving

rates, which seems to be due to differences in water densities, upwelling turbulent heat transfers and underwater melting rates, among others.

Not all the calving laws have been written as a function of the water depth. Other works, such as Sikonia (1982), have attempted to write down calving laws in terms of the height of the terminal ice cliff above buoyancy h_0. This represents the excess height with respect to a free floating ice body in the same water and is defined as

$$h_0 = h_i - \frac{\rho_w}{\rho_i} h_w. \tag{50}$$

2.3 Tidewater glacier cycles

The dependence of the calving rate on the water column depth is thought to play a crucial role in tidewater glacier cycles. Observations and paleoclimate proxies suggest that in warmer climates tidewater glaciers tend to undergo catastrophic retreats. For example, the Columbia glacier was observed to retreat about 12 km between 1982 and 2002. To explain that, the following simple reasoning has been developed. Let us start from a condition in which the calving front is in a fixed position set by balance between the inflow mass and the mass loss due to calving and melting. If at some point the up-glacier dynamics start pushing the front further, a moraine shoal develops at the base of the front and the calving rate reduces because of the decrease of the effective water depth at the glacier front. In this way, the glacier is able to advance because the height of the moraine increases and keeps the calving rate low. This is hypothesized to be sustainable for up to 1000 y at a rate of order 30 m y^{-1} (Meier and Post, 1987). If then, perhaps due to inherent instability of the steady state, the glacier starts retreating, it finds itself in contact with the full water column depth, with no moraine shielding it, and the calving rate suddenly increases, causing the front to retreat further. The retreat stops when the water column is shallow enough to return to a quasi-stable equilibrium between inflow and mass loss at the front. This kind of retreat is thought to happen over scales of 100 y at a rate of order 1 km y^{-1} and figure 4 shows a schematic of it.

Another feedback loop that might explain the initiation and the sudden retreat of the tidewater glaciers described above has been has been hypothesized for the relationship between thinning, acceleration and calving retreat by Benn et al. (2007). In particular, this study affirms that an increase in surface melting drives the thinning of the glacier, which is responsible for a reduced effective pressure and a consequent increase in velocity and longitudinal strain rate. First, this generates dynamic thinning, leading to a further decrease in effective pressure. Second, this process leads to deeper crevasses, which causes the calving margin to retreat more quickly.

3 Conclusion: A Cautionary Tale

As a conclusion, Dr. Fowler warned the theorists among us not to get too enamoured of theory, to the exclusion of its application:

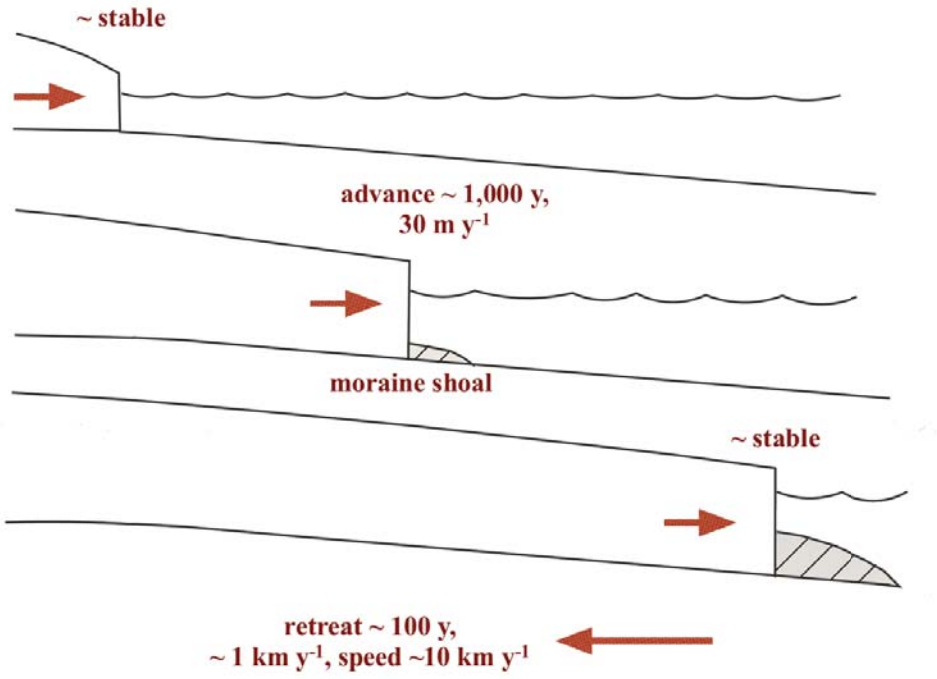

Figure 4: Schematic of the tidewater glacier cycle.

"Pfuel was one of those theorists who so love their theory that they forget the purpose of the theory - its application in practice; in his love for theory, he hated everything practical and did not want to know about it. He was even glad of failure, because failure, proceeding from departures from theory in practice, only proved to him the correctness of his theory." Tolstoy, War and Peace, III, I, X.

References

Benn, D. I., Warren, C. R., and Mottram, R. H. (2007). Calving processes and the dynamics of calving glaciers. *Earth-Science Reviews*.

Creyts, T. T. and Schoof, C. G. (2009). Drainage through subglacial water sheets. *Journal of Geophysical Research*, 114(F4):F04008.

Fowler, A. (2011). *Mathematical Geoscience*, volume 36 of *Interdisciplinary Applied Mathematics*. Springer London, London.

Haresign, E. C. (2004). *Glacio-limnological interactions at lake-calving glaciers*. PhD thesis, University of St Andrews.

Kirchner, N., Ahlkrona, J., Gowan, E., Lötstedt, P., Lea, J., Noormets, R., von Sydow, L., Dowdeswell, J., and Benham, T. (2016). Shallow ice approximation, second order shallow

ice approximation, and full stokes models: A discussion of their roles in palaeo-ice sheet modelling and development. *Quaternary Science Reviews*, 147(Supplement C):136 – 147. Special Issue: PAST Gateways (Palaeo-Arctic Spatial and Temporal Gateways).

Kyrke-Smith, T. M., Katz, R. F., and Fowler, A. C. (2013). Subglacial hydrology and the formation of ice streams. *Proceedings of the Royal Society A: Mathematical, Physical and Engineering Sciences*, 470(2161):20130494–20130494.

Meier, M. F. and Post, A. (1987). Fast tidewater glaciers. *Journal of Geophysical Research*, 92(B9):9051–9058.

Meur, E. L., Gagliardini, O., Zwinger, T., and Ruokolainen, J. (2004). Glacier flow modelling: a comparison of the shallow ice approximation and the full-stokes solution. *Comptes Rendus Physique*, 5(7):709 – 722. Ice: from dislocations to icy satellites.

Nye, J. F. (1957). The Distribution of Stress and Velocity in Glaciers and Ice-Sheets. *Proceedings of the Royal Society A: Mathematical, Physical and Engineering Sciences*, 239(1216):113–133.

Sikonia, W. G. (1982). Finite-element glacier dynamics model applied to Columbia glacier, Alaska. *U. S. Geol. Surv. Prof. Pap.*, 1258-B.